Title

Mechanism of gating by calcium in connexin hemichannels

Journal

Proceedings of the National Academy of Sciences of the United States of America, 113(49)

ISSN

0027-8424

Authors

Lopez, William
Ramachandran, Jayalakshmi
Alsamarah, Abdelaziz
et al.

Publication Date

2016-12-06

DOI

10.1073/pnas.1609378113

Peer reviewed

Mechanism of gating by calcium in connexin hemichannels

William Lopez[a], Jayalakshmi Ramachandran[a], Abdelaziz Alsamarah[b], Yun Luo[b], Andrew L. Harris[a], and Jorge E. Contreras[a,1]

[a]Department of Pharmacology, Physiology and Neuroscience, New Jersey Medical School, Rutgers University, Newark, NJ 07103; and [b]Department of Pharmaceutical Sciences, College of Pharmacy, Western University of Health Sciences, Pomona, CA 91766

Edited by Richard W. Aldrich, The University of Texas at Austin, Austin, TX, and approved November 2, 2016 (received for review June 9, 2016)

Aberrant opening of nonjunctional connexin hemichannels at the plasma membrane is associated with many diseases, including ischemia and muscular dystrophy. Proper control of hemichannel opening is essential to maintain cell viability and is achieved by physiological levels of extracellular Ca^{2+}, which drastically reduce hemichannel activity. Here we examined the role of conserved charged residues that form electrostatic networks near the extracellular entrance of the connexin pore, a region thought to be involved in gating rearrangements of hemichannels. Molecular dynamics simulations indicate discrete sites for Ca^{2+} interaction and consequent disruption of salt bridges in the open hemichannels. Experimentally, we found that disruption of these salt bridges by mutations facilitates hemichannel closing. Two negatively charged residues in these networks are putative Ca^{2+} binding sites, forming a Ca^{2+}-gating ring near the extracellular entrance of the pore. Accessibility studies showed that this Ca^{2+}-bound gating ring does not prevent access of ions or small molecules to positions deeper into the pore, indicating that the physical gate is below the Ca^{2+}-gating ring. We conclude that intra- and intersubunit electrostatic networks at the extracellular entrance of the hemichannel pore play critical roles in hemichannel gating reactions and are tightly controlled by extracellular Ca^{2+}. Our findings provide a general mechanism for Ca^{2+} gating among different connexin hemichannel isoforms.

connexin | hemichannels | gating

Unapposed connexin hemichannels are found at the plasma membrane before docking with hemichannels of apposed cells to form intercellular gap junction channels. Under normal physiological conditions, hemichannel activity at the surface is tightly regulated to be null or very low. This is important for maintaining the electrochemical gradient across the plasma membrane, because hemichannels are relatively nonselective among atomic ions. There is growing evidence, however, that transient or controlled opening of unapposed hemichannels plays physiological roles in various cell types by release to the external milieu of small cytoplasmic metabolites (i.e., glutamate, glutathione, ATP) (1, 2). It is widely accepted that hyperactive connexin hemichannels play pathological roles. For instance, several human connexin mutations that cause human pathologies produce exacerbated hemichannel activity at the plasma membrane, which has deleterious consequences (3–5). Similarly, in nongenetic pathologies, including ischemia and muscular dystrophy, there is strong evidence that opening of hemichannels enhances tissue damage (6–8). Understanding the mechanisms that control the activity of unapposed hemichannels is biomedically important.

A major regulator of hemichannel activity under physiological conditions is extracellular Ca^{2+}, which at normal levels (~1.8 mM) keeps open probability very low. Reduction of extracellular Ca^{2+} increases the opening of most, if not all, unapposed connexin (Cx) hemichannels (i.e., Cx26, Cx32, Cx43, Cx46, Cx50) (9–17). Unlike most other ion channels regulated by Ca^{2+}, connexin channels do not have a large semiindependent structural domain that binds Ca^{2+} and couples allosterically to the pore to control opening and closing. This type of Ca^{2+}-binding domain at the extracellular face of connexin hemichannels is not feasible, because it would interfere with the formation of intercellular gap junction channels. Most likely, Ca^{2+} sensing is predominantly mediated by motifs that lie within or are exposed to the pore lumen (18).

Recently, we found that extracellular Ca^{2+} destabilizes the open state of hemichannels, at least in human Cx26 (hCx26) and hCx30, by disrupting a salt-bridge interaction between residues D50 and K61 located close to the extracellular entrance of the pore (17, 19). This open-state destabilization facilitates hemichannel closure (17, 19). However, disruption of this interaction does not seem to be a general mechanism for Ca^{2+} regulation of connexins, because these charges at these positions are not highly conserved across the family of connexin proteins. hCx26 crystal structure (20) and molecular dynamics studies (21) suggest a highly conserved electrostatic network located at the extracellular entrance of the pore in all connexin types that is involved in gating. In the present work, we found that extracellular Ca^{2+} directly and/or indirectly disrupts the open-channel form of this network to favor a closed conformation. We conclude that negatively charged residues lining the pore that are part of this electrostatic network play critical roles in hemichannel gating reactions and seem critical for Ca^{2+} binding but do not constitute the closed hemichannel gate.

Results

Calcium Disrupts Electrostatic Networks at the Extracellular Pore Entrance to Facilitate Hemichannel Closure. We previously reported that two charged residues (D50 and K61) at the extracellular end of the Cx26 hemichannel pore form a salt-bridge interaction that

Significance

Connexin channels are ubiquitous, providing pathways for movement of molecules between cells (junctional channels) and for release of molecular effectors into the extracellular environment (plasma membrane hemichannels). To maintain an adequate permeability barrier, hemichannels are tightly regulated by normal extracellular Ca^{2+} to be closed under most conditions. Connexin mutations that disrupt hemichannel regulation by Ca^{2+} cause human pathologies due to aberrantly open hemichannels. Here we elucidate molecular mechanisms of gating by Ca^{2+} in hemichannels: Ca^{2+} binding causes a reorganization of specific interactions within the connexin protein that lead to a closed channel. Further, we show that the actual "gate" is deeper into the pore from where Ca^{2+} binds. The interactions involved are conserved across connexins, pointing to a general mechanism.

Author contributions: J.E.C. designed research; Y.L. designed the molecular dynamics simulations; W.L., J.R., A.A., and J.E.C. performed research; A.A. and Y.L. performed the molecular dynamics simulations; A.L.H. provided guidance for molecular dynamics design and interpretations; W.L., J.R., and J.E.C. analyzed data; and Y.L., A.L.H., and J.E.C. wrote the paper.

The authors declare no conflict of interest.

This article is a PNAS Direct Submission.

[1]To whom correspondence should be addressed. Email: contrejo@njms.rutgers.edu.

This article contains supporting information online at www.pnas.org/lookup/suppl/doi:10.1073/pnas.1609378113/-/DCSupplemental.

stabilizes the hemichannel in the open state (Fig. 1 *A* and *B*). We proposed that this interaction is disrupted with increasing extracellular Ca^{2+} concentrations, and that this may constitute the initial reaction for hemichannel closure (17). To gain further insights into the gating mechanism mediated by Ca^{2+} disruption of the D50–K61 interaction, we performed molecular dynamics simulations, building on previously well-established equilibrated structures of Cx26 hemichannels (22, 23). We observed that K^+ ions accumulate near the extracellular entrance of the pore where several negatively charged residues are located, including D50 (23). In the model, we replaced six of the K^+ ions that were at or just external to the extracellular end of the channel with Ca^{2+} ions (Fig. S1*A*) and performed simulations of up to 50 ns. In the simulations, two of the Ca^{2+} ions interacted rapidly with D50 side chains in two of the connexin subunits (chains A and E; Fig. 1*C*, red and black spheres, respectively), consistent with previous experimental data identifying this residue as a key player in Ca^{2+} regulation of this channel (17). These Ca^{2+} ions remained bound to the D50 residues throughout the simulation (see Fig. S1*B* for depiction of the Ca^{2+} ion locations during the simulation). Also consistent with experimental findings, the D50 interaction with Ca^{2+} disrupted the intersubunit salt-bridge interaction of the D50 residues with K61 in the adjacent subunit (between chains A and B and between chains E and F; Fig. 1*D*, black and red traces, respectively).

The D50–K61 salt bridge is near an extensive network of electrostatic interactions (Fig. 2*A*) at the external entrance of the pore that is highly conserved among different connexins (Fig. S2). It has been proposed that reorganization of this network plays a key role in gating (21). The molecular dynamics simulations show that the electrostatic network involving these residues is rearranged in

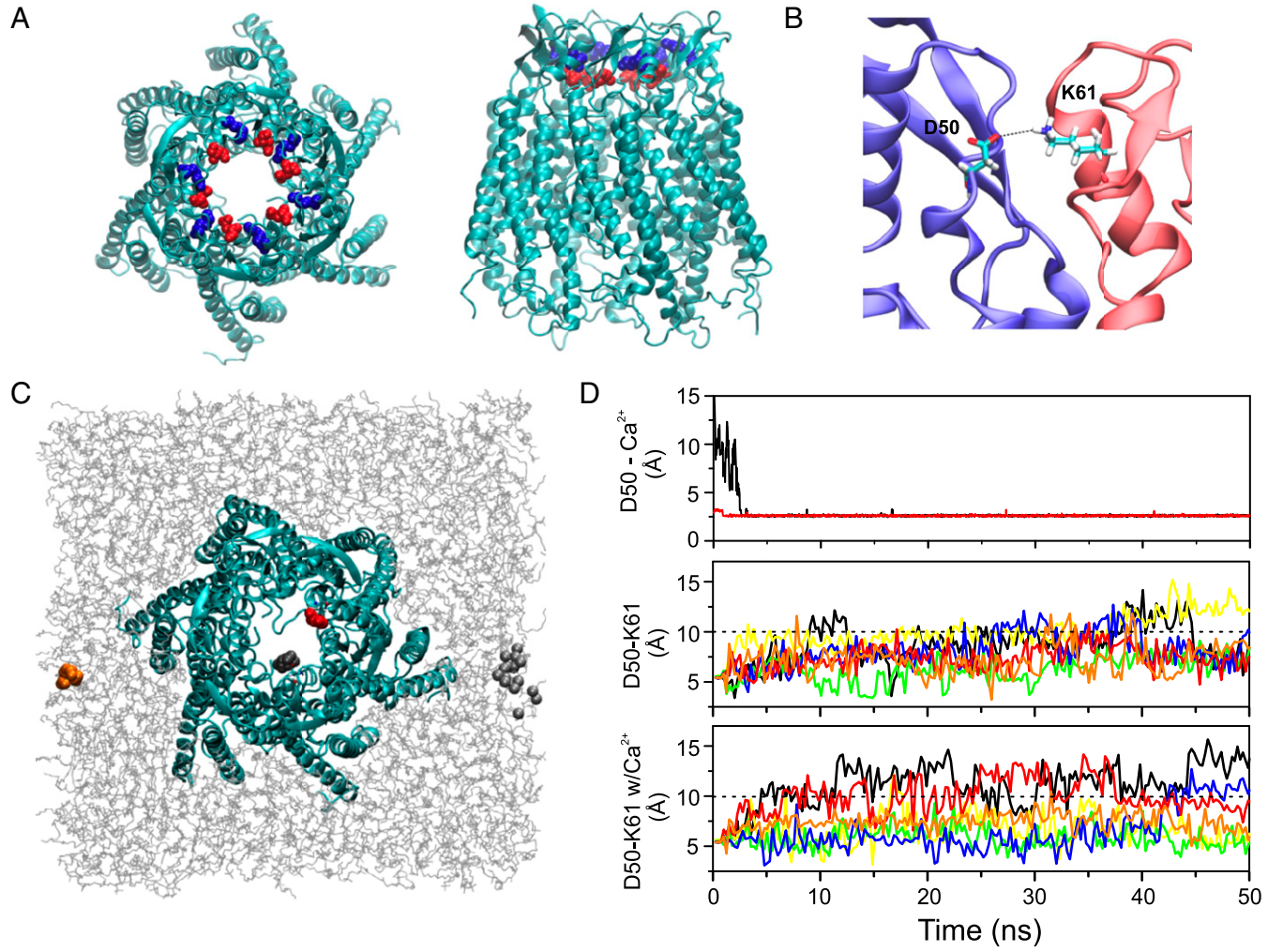

Fig. 1. Molecular dynamics (MD) simulations show interaction of Ca^{2+} ions with residue D50 accompanied by loss of interaction between residues D50 and K61. (*A*) Top (*Left*) and side views (*Right*) of the Cx26 hemichannel showing D50 (red) and K61 (blue) at the extracellular entrance of the pore, which form intersubunit salt bridges. (*B*) Close-up view of the intersubunit salt bridge between D50 and K61. (*C*) Extracellular view of the simulation cell showing the Cx26 hemichannel and the lipid bilayer, following introduction of six Ca^{2+} ions and MD simulations. The Ca^{2+} ions are shown as van der Waals (vdW) balls superimposed for every 2.0 ns of the last 30 ns of a 50-ns simulation. Two Ca^{2+} ions (red and black) rapidly coordinated with residue D50 of chains A and E, where they remained for the duration of the simulation. Two Ca^{2+} ions (orange and gray) became bound to lipid head groups, and two Ca^{2+} ions drifted away. The initial positions of the six Ca^{2+} ions and snapshots during the simulations are shown in Fig. S1. Phospholipids are depicted in line format. Water, Cl^-, and K^+ ions are not shown. (*D*) Distances between the side chain of residue D50 and Ca^{2+} (*Top*) and between the side chains of D50 and K61 during MD simulations without (*Middle*) and with (*Bottom*) Ca^{2+} for each intersubunit D50–K61 interaction. (*D*, *Top*) Nearly immediate coordination of Ca^{2+} by D50 of chain E (red) and coordination of Ca^{2+} by D50 of chain A within 3 ns of the start of simulation (black). (*D*, *Middle* and *Bottom*) With Ca^{2+} coordination by the D50 residues of chains A and E, the intersubunit D50–K61 distances significantly and specifically increase for interactions involving those D50 residues (red and black). Distances are measured between the D50Cγ and K61Nζ atoms. Black, subunits A_{D50}–B_{E61}; yellow, subunits B_{D50}–C_{E61}; green, subunits C_{D50}–D_{E61}; blue, subunits D_{D50}–E_{E61}; red, subunits E_{D50}–F_{E61}; brown, subunits F_{D50}–A_{E61}.

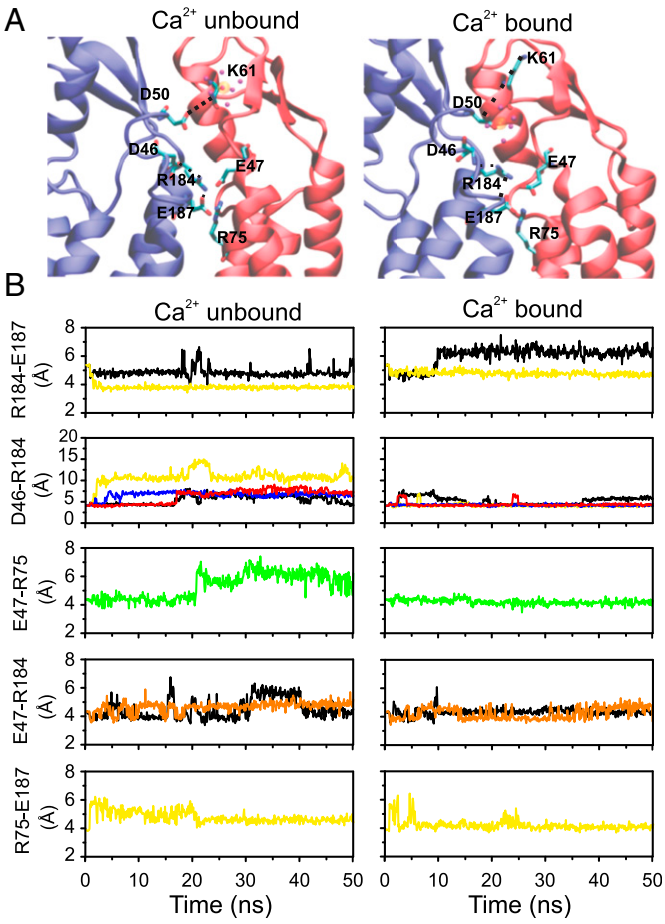

Fig. 2. Electrostatic network at the entrance of the pore is altered when Ca^{2+} interacts with D50. (*A*) Electrostatic network of the Cx26 hemichannel model formed by residues D46, E47, R75, R184, and E187 before (*Left*) and after (*Right*) Ca^{2+} is coordinated at position D50, after 50-ns molecular dynamics simulations. Ca^{2+} ions are depicted as small orange spheres. Also note the increased K50–K61 distance with Ca^{2+} bound. (*B*) Distances between the side chains of intrasubunit residue pairs R184–E47, D46–R184, and E47–R75, and intersubunit residue pairs E47–R184 and R75–E187, during 50-ns MD simulations without (*Left*) and with (*Right*) Ca^{2+}. Only interactions that changed significantly following Ca^{2+} coordination during the MD simulations are shown. The complete dataset depicting these interactions as well as the ones that did not change are shown in Fig. S3. For intrasubunit interactions, distances were measured between atoms R184Cζ and E187Cδ, D46Cγ and R184Cζ, and E47Cδ and R75Cζ. For intersubunit interactions, distances were measured between atoms E47Cδ and R184Cζ, and R75Cζ and E187Cδ. Intrasubunit interactions (R184–E47, D46–R184, E47–R75): black, subunit A; yellow, subunit B; green, subunit C; blue, subunit D; red, subunit E; brown, subunit F. Intersubunit interactions (E47–R184, R75–E187): black, subunits A–B; yellow, subunits B–C; green, subunits C–D; blue, subunits D–E; red, subunits E–F; brown, subunits F–A.

several subunits in response to Ca^{2+} coordination by D50 in two subunits. As a result of Ca^{2+} coordination at D50 of subunits A and E and the concomitant loss of D50 interactions with K61 in subunits B and F, respectively (shown in Fig. 1), several qualitative changes occur in other interactions in the same and other subunits within the 50-ns computational time frame. These are shown in Fig. 2*B* (the complete dataset for all interactions and all subunits is shown in Fig. S3). Some interactions are weakened (longer distances) and some are strengthened (shorter distances). The most dramatic changes observed in the presence of Ca^{2+} are a weakening of the intrasubunit R184–E187 interaction in subunit A and a strengthening of the intrasubunit interactions D46–R184 and E47–R75 in chains B and C, respectively. More subtle changes occur at other sites and other subunits.

The breaking of the R184–E187 interaction (chain A) suggests this interaction as a candidate for stabilizing the open state. Beyond this, one cannot distinguish between changes that compensate for the loss of stabilization of the open state produced by Ca^{2+} disruption of D50–K61 and the subsequent loss of R184–E187, or changes involved in progression toward formation of a Ca^{2+}-closed state.

These simulations suggest that the electrostatic network near the extracellular end of the pore undergoes significant disruption/rearrangement even within a 50-ns simulation time frame. These changes are properly regarded as potential initial changes induced by Ca^{2+} interaction with D50 and the direct disruption of the D50–K61 interaction. These changes extend deeper into the pore than the site of Ca^{2+} coordination, and involve subunits (and residues) not directly involved in Ca^{2+} coordination.

To experimentally investigate the role of this conserved electrostatic network, we introduced single mutations at sites suggested by the molecular dynamics simulations and evaluated the changes in deactivation kinetics as a function of Ca^{2+} concentration. We used a standard protocol for assessment of hCx26 hemichannel activation and deactivation via examination of the peak tail currents and their relaxation kinetics following 40-s pulses from −80 to 0 mV (17). Unfortunately, most of the tested mutations led to nonfunctional channels. Only a few positions allowed specific mutations that could be experimentally tested; these mutations were D46C, E47Q, D50N, and R184K. Fig. 3 *A*–*E* shows current traces obtained at different Ca^{2+} concentrations for oocytes expressing wild-type and mutant hemichannels.

As previously shown (17), the tail current deactivation kinetics of wild-type hCx26 hemichannel closure becomes slower when the extracellular Ca^{2+} concentration is reduced. This indicates that with lowering of the Ca^{2+} concentration the dominant barrier to channel closing becomes greater, relative to the barrier to opening. Oocytes expressing the mutants D50N, E47Q, D46C, or R184K showed faster deactivation kinetics at low Ca^{2+} concentrations compared with wild-type Cx26 (Fig. 3 *B*–*F*), suggesting a reduced barrier to closing. In addition to these kinetic effects, three of the mutations (D50N, E47Q, D46C) essentially eliminated the Ca^{2+} dependence of the tail current relaxations, whereas one of them (R184K) retained some degree of Ca^{2+} dependence (Fig. 3*F*). Together, these results suggest that the effect of Ca^{2+} on hemichannel closing is mediated by relative destabilization of the open state involving disruption of (likely electrostatic) interactions of these mutated residues.

Two Negatively Charged Residues at the Pore Are Critical for Regulation by Ca^{2+}. To gain additional mechanistic insight, the steady-state Ca^{2+} dose–response relations of the functional mutants were examined. The normalized peak tail currents as a function of Ca^{2+} concentration are shown in Fig. 4*A*. The Ca^{2+} dose–response relations were fit to a Hill equation of the form

$$I/I_{max} = 1/\left(1 + \left[Ca^{2+}\right]/K_D\right)^n, \quad [1]$$

where the fractional current is I/I_{max}, I is the peak tail current at a particular Ca^{2+} concentration, I_{max} is the maximal tail current at 0.01 mM Ca^{2+}, K_D is the apparent affinity, $[Ca^{2+}]$ is the concentration of Ca^{2+}, and n is the Hill coefficient. The estimated values for K_D and n of wild-type Cx26 hemichannels are 0.33 mM and 1.38, respectively. For the mutations that replaced negatively charged residues with uncharged residues, D46C mutants did not show a change in apparent Ca^{2+} sensitivity compared with wild type but D50N and E47Q mutants showed a significant rightward shift, consistent with decreased Ca^{2+} binding and/or decrease of open-state energy relative to the closed state. D50N also has a

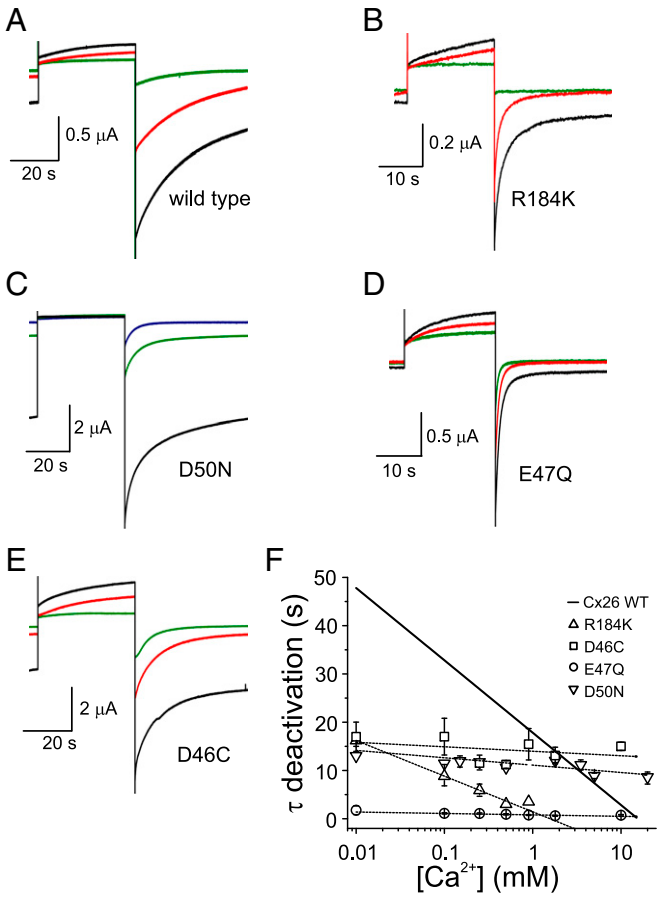

Fig. 3. Mutations within the extracellular network accelerate deactivation kinetics in Cx26 hemichannels. Tail currents were assessed following a 40-s pulse to 0 mV from a holding potential of −80 mV. (*A*) Representative current traces for an oocyte expressing wild-type Cx26 hemichannels at three different Ca^{2+} concentrations (1.8 mM, green; 0.5 mM, red; 0.1 mM, black). (*B*) Current traces for an oocyte expressing R184K obtained as described in *A*. (*C*) Current traces for an oocyte expressing D50N mutant hemichannels at three different Ca^{2+} concentrations (3.5 mM, blue; 1.8 mM, green; 0.1 mM, black). (*D* and *E*) Current traces for oocytes expressing E47Q and D46C, respectively, obtained as described in *A*. (*F*) Deactivation time constants of the corresponding tail currents at different Ca^{2+} concentrations for R184K, D50N, E47Q, and D46C. Dotted lines are the best linear fits to the mutant hemichannel data. The solid line corresponds to the linear fit of the average data for wild-type hemichannels [data are from Lopez et al. (17)]. The data represent mean ± SEM of at least five independent measurements. Significant differences were observed for D50N, D46C, R184K, and E47Q compared with wild type ($P < 0.001$ for the first two and $P < 0.01$ for the latter two).

decreased slope, which suggests, in addition, a reduced effect of Ca^{2+} binding energy on the relative energies of the open and closed states from in wild type or E47Q mutants, consistent with the Ca^{2+} interaction with D50 indicated by the molecular dynamics simulations. The best-fit parameter values for K_D and n were 0.34 mM and 0.86 for D46C, 1.11 mM and 1.68 for E47Q, and 1.31 mM and 0.7 for D50N. Conversely, the mutant R184K showed a leftward shift, consistent with a change in the electrostatic interactions of this position that increased Ca^{2+} binding affinity and/or increased closed-state energy relative to the open state; the values for K_D and n are 0.15 mM and 1.31, respectively.

Because mutations at positions D50 and E47 each showed a significant decrease in the apparent Ca^{2+} affinity, we attempted to create a D50/E47 double mutant to potentially generate a more significant effect on Ca^{2+} sensitivity. A greater effect of the double mutant than that produced by each individual mutation would suggest some degree of independent contributions of the interactions of D50 and E47 to Ca^{2+} regulation of the channel. Although several combinations of mutated residues were tested, none yielded functional hemichannel currents. Because these negatively charged residues are highly conserved in many other connexins, we chose to perform the analogous experiments in Cx46 hemichannels, as they have been shown to be amenable for electrophysiological and mutagenesis studies. Residues E47 and D50 in Cx26 correspond to residues E48 and D51 in Cx46. We introduced mutations at these sites, substituting aspartate and glutamate with the neutral amino acids glutamine and asparagine, respectively. Cx46 hemichannel activation was assessed by the peak tail currents following a 20-s pulse from −80 to 20 mV at different Ca^{2+} concentrations (Fig. S4*A*; a modified protocol was used because of different activation properties of Cx46 relative to Cx26).

Fig. 4*B* shows the $[Ca^{2+}]$ dose–response relations for Cx46 wild type and mutants. Over a concentration range of 0.1 to 10 mM extracellular Ca^{2+}, wild-type Cx46 hemichannels showed only slightly less apparent affinity for Ca^{2+} than Cx26 (K_D 0.6 mM vs. 0.33 mM). Strikingly, the single mutants E48Q and D51N showed the same effects on Cx46 Ca^{2+} dependence as seen for the corresponding mutations in Cx26 (E48Q: shifted right with the same slope, similar to E47Q in Cx26; D51N: shifted right with reduced slope, similar to D50N in Cx26). The calculated values for K_D for E48Q and D51N mutants were 1.1 and 3 mM, respectively. Thus, the mutations in the Cx46 system reproduce effects similar to those seen in Cx26 regarding changes in Ca^{2+} dose–response relations for the single mutants E48Q and D51N.

The successful E48Q/D51N double mutant in Cx46 greatly reduces Ca^{2+} sensitivity. The best-fit parameter values for K_D and n from the $[Ca^{2+}]$ dose–response curves for the double mutant E48Q/D51N were 8 mM and 1.3, respectively. This suggests that the interactions involving each of the mutated residues contribute to the Ca^{2+} sensitivity, reinforcing the idea that a network of interactions involving these residues mediates the Ca^{2+} regulation.

In addition, the E48Q/D51N double mutants showed high "leak" currents at negative holding potentials, consistent with decreased regulation by Ca^{2+} (Fig. S4*B*). Thus, we evaluated the current–voltage relationship for wild-type and E48Q/D51N double mutant hemichannels. At physiological Ca^{2+} concentrations, Cx46 wild-type hemichannels activate only at potentials more positive than 0 mV (Fig. 4*C*, black circles). In contrast, oocytes injected with E48Q/D51N double mutants show hemichannel currents at negative potentials (Fig. 4*C*, red circles). A hyperpolarizing pulse from −10 to −100 mV reveals that oocytes expressing the E48Q/D51N double mutant display multiphasic inward currents, including currents typically mediated by Ca^{2+}-activated chloride channels (Fig. 4*D*). BAPTA (1,2-bis(*o*-aminophenoxy)ethane-*N*,*N*,*N*′,*N*′-tetraacetic acid) injections prevent these chloride currents and result in monophasic currents, suggesting that Ca^{2+} influx via E48Q/D51N mutants activated these chloride channels (Fig. S5). As expected for a cell expressing leaky hemichannels, oocytes containing E48Q/D51N mutants begin to die within 48 h after mRNA injections (Fig. 4*E*).

Together, our data suggest that the electrostatic interactions of residues D50 and E47 in Cx26, and the corresponding residues D51 and E48 in Cx46, are major contributors to the stability of the closed state that is produced by interaction with Ca^{2+}.

The Calcium-Bound Ring Does Not Form a Tight Gate. A recent crystal structure of Cx26 gap junction channels (docked hemichannels) also indicates that E47 residues directly participate in Ca^{2+} coordination and the formation of a Ca^{2+}-bound sensing ring at the entrance of the pore (18). Calculations based on this structure indicated that the Ca^{2+}-bound sensing ring forms an electrostatic gate that restricts occupancy of the channel by cations in gap junction channels (18).

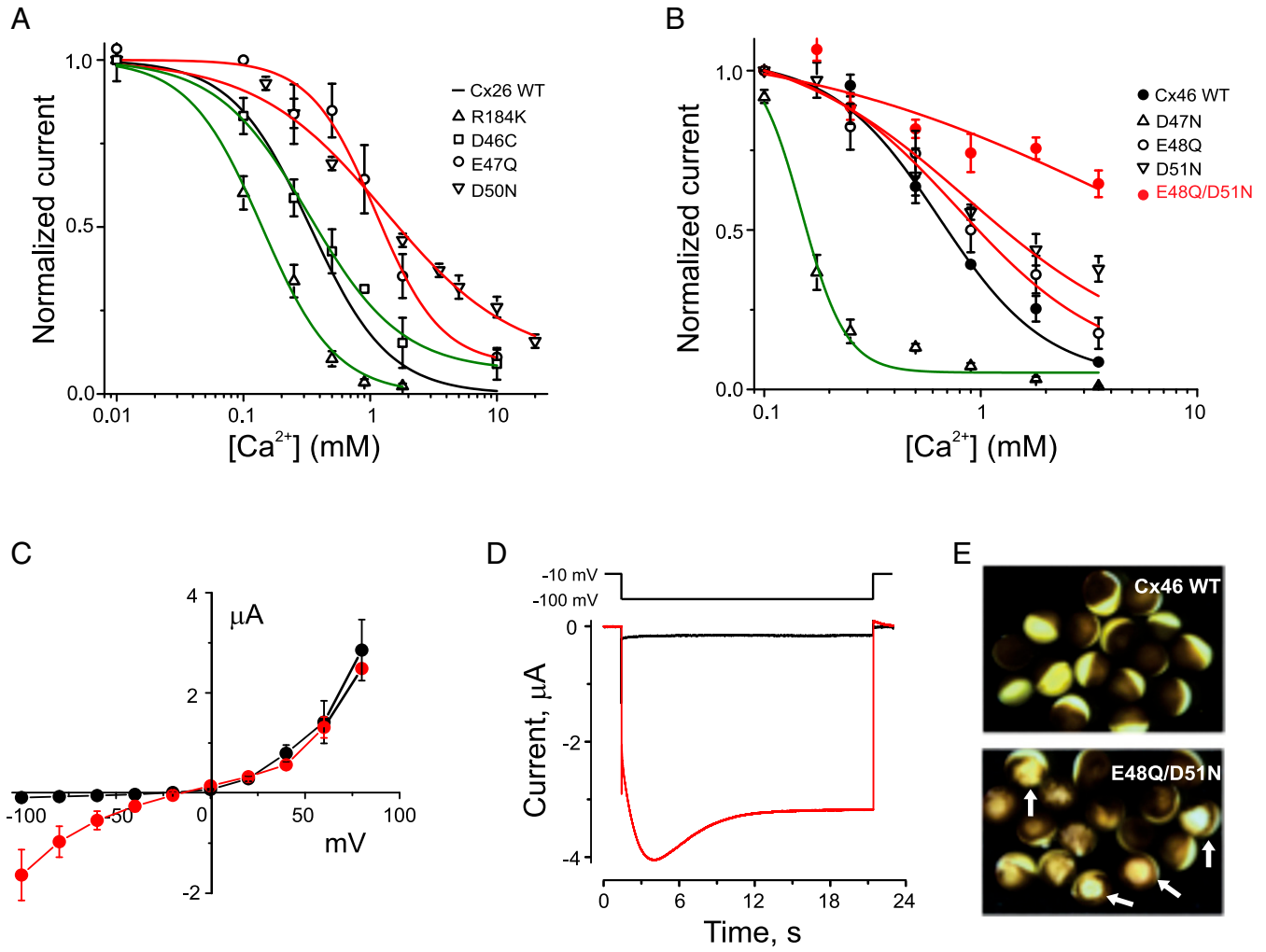

Fig. 4. Negatively charged residues D50 and E47 in Cx26 hemichannels and D51 and E48 in Cx46 are key players in Ca^{2+} regulation. (*A*) Ca^{2+} dose–response curve for oocytes expressing wild-type Cx26 and R184K, D46C, E47Q, and D50N mutant hemichannels. The black line represents best fits to a Hill equation (Eq. **1**) for wild type [data are from Lopez et al. (17)]. Red lines are fits to the data for mutations that decrease Ca^{2+} sensitivity (E47Q and D50N). Green lines are fits to the data for mutants that do not change (D46C) or increase (R184K) Ca^{2+} sensitivity. The data represent mean ± SEM of at least three independent measurements. Significant differences were observed for apparent affinities of R184K, D50N, and E47Q compared with wild type ($P < 0.01$ for each) but not for the apparent affinity between D46C and wild type. (*B*) Ca^{2+} dose–response curve for oocytes expressing Cx46 wild-type and D47N, E48Q, and D51N single mutant hemichannels and the E48Q/D51N double mutant. Red lines are fits to the data for mutations that decrease Ca^{2+} sensitivity (E48Q, D51N, and D48Q/D51N). Green lines are fits to the data for mutants that do not change (D46C) or increase (R184K) Ca^{2+} sensitivity. Significant differences were observed for apparent affinities of D47N, D51N, and the E48Q/D51N double mutant compared with wild type ($P < 0.001$ for the first two and $P < 0.01$ for the last). The comparison of the E48Q with wild type did not reach statistical significance ($P = 0.065$), although there is a trend toward a difference. The data represent mean ± SEM of at least three independent measurements. (*C*) Current–voltage relationship for Cx46 wild type (black) and the double mutant D51N/E48Q (red). Injected oocytes were held at −80 mV and voltage steps were applied from −100 mV every 20 mV followed by a test pulse to −80 mV. The data represent mean ± SEM of at least three independent measurements. (*D*) Leak currents during a hyperpolarizing pulse to −100 mV from a holding potential of −10 mV in an oocyte expressing Cx46 wild-type (black) or D51N/E48Q (red) hemichannels. (*E*) Images showing the damaging effect on oocytes (arrows) expressing Cx46 D51N/E48Q hemichannels (*Lower*) compared with wild-type hemichannels (*Upper*) 48 h after mRNA injections.

To test the possibility that such a Ca^{2+}-gating ring, involving D50 and E47, is the physical gate of Cx26 hemichannels, we evaluated the extracellular accessibility of MTSES (2-sulfonatoethyl methanethiosulfonate) to a substituted cysteine at position G45 in the presence of different Ca^{2+} concentrations. The G45C mutation is located below the Ca^{2+}-gating ring (Fig. 5*A*). We and others have shown that MTSES modification of the G45C mutant augments hemichannel currents, whereas application of MTSES to wild-type Cx26 hemichannels is without effect (24, 25). Using previously well-characterized protocols (24), we assessed tail current peaks in the absence and presence of MTSES after reaching current saturation during a depolarizing pulse from −80 to 0 mV. Following application of MTSES there is a dramatic increase in the tail current mediated by G45C mutant hemichannels (Fig. 5*B*). Single exponential fits to the tail currents allow estimation of the rate of modification (Fig. 5*C*). To evaluate whether the rate of MTSES modification of G45C correlated with hemichannel opening at different Ca^{2+} concentrations, the modification rates obtained at 0.1, 0.25, and 1.8 mM extracellular Ca^{2+} were plotted for comparison with normalized current values obtained at different Ca^{2+} concentrations (Fig. 5*D*). At all Ca^{2+} concentrations and despite the large changes in hemichannel currents due to MTSES modification, the modification rates were essentially unchanged (~50 $M^{-1}{\cdot}s^{-1}$). Thus, these results indicate that the MTSES modification rate of G45C is independent of the extracellular Ca^{2+} concentration and

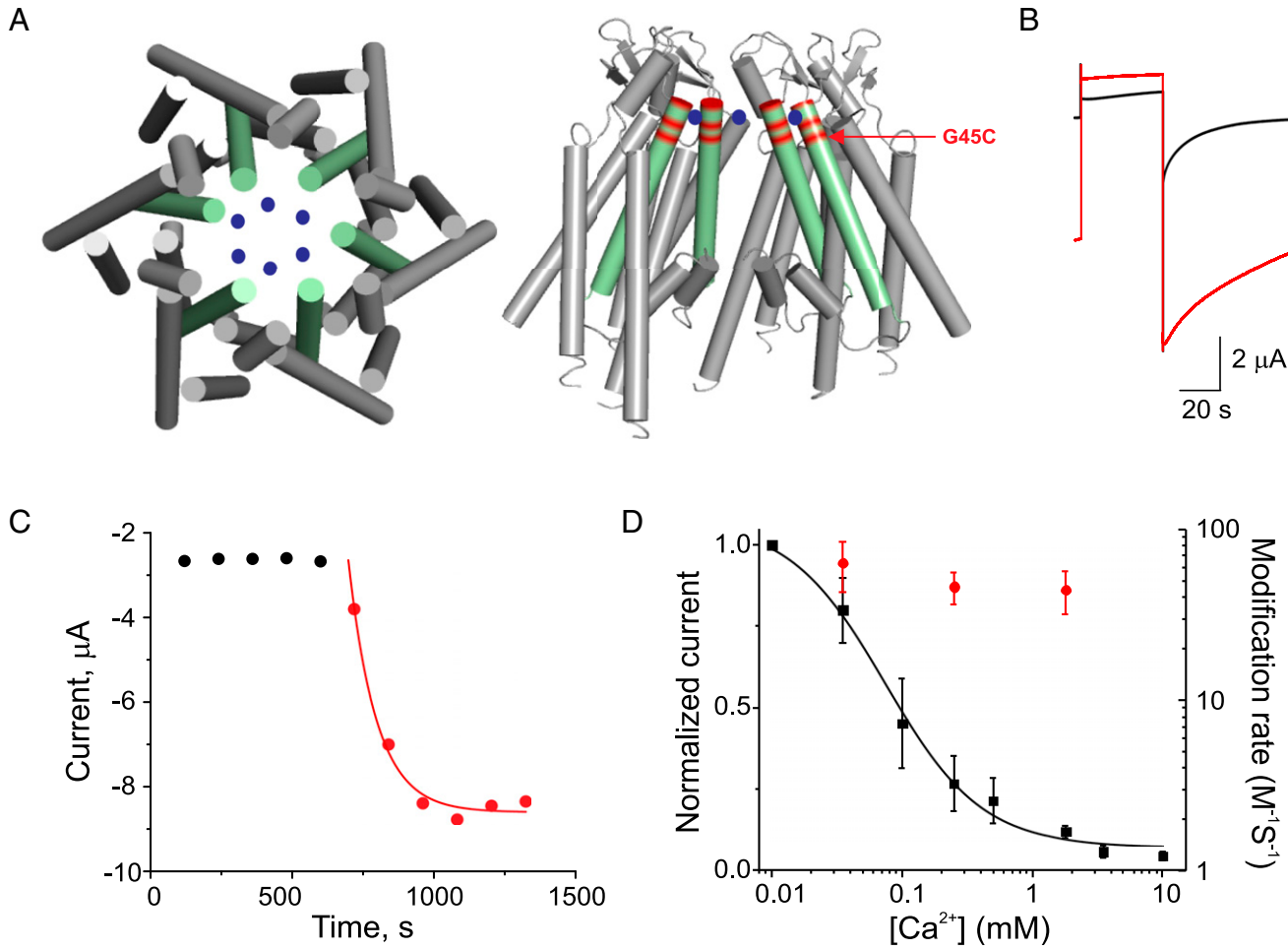

Fig. 5. MTSES accessibility to G45C, a site below D50/E47, is independent of extracellular Ca^{2+} concentration. (*A*) Top (*Left*) and side view (*Right*) representation of the Cx26 hemichannel structure indicating the position of Ca^{2+} interaction (D50/E47) at the extracellular entrance of the pore and the location of position G45C. In the side view, the two closest subunits are not shown, to expose the pore-lining region. Approximate Ca^{2+} locations are indicated by blue spheres. Residues D50, E47, and G45 are highlighted in red. (*B*) Representative current traces from an oocyte expressing G45C mutant hemichannels before (black line) and after (red line) modification with 500 μM MTSES. The current traces were obtained in response to a depolarizing pulse to 0 mV from a holding potential of −80 mV in the presence of 0.25 mM extracellular Ca^{2+}. (*C*) Time course of the increase in peak tail currents of G45C mutants in the absence (black circles) and presence (red circles) of MTSES. The red line is a single exponential fit to the increase in peak tail currents following MTSES application. (*D*) Comparison of the modification rate of G45C by MTSES (red circles) and normalized peak tail currents (black squares) as functions of Ca^{2+} concentration. The data represent mean ± SEM of at least three independent measurements.

channel closure by Ca^{2+}; accessibility to G45C by MTSES is unaffected by Ca^{2+} gating of Cx26 hemichannels, despite being below the Ca^{2+}-gating ring.

The observed modification rate, however, is relatively slow, which indicates restricted access of MTSES to G45C. Because it is well-established that G45C lines the aqueous pore, one possible explanation is that G45C is below a nongating physical or electrostatic barrier (but not a gate) that affects access in a state-independent manner. To further rule out the absence of a gate at the Ca^{2+}-gating ring region, we examined the extracellular accessibility of Cd^{2+} to G45C. Oocytes expressing wild-type or G45C mutant hemichannels were held at 5 mV and then exposed to rapid perfusion of 1 μM Cd^{2+}. In wild-type channels, 1 μM Cd^{2+} had essentially no effect at Ca^{2+} levels of 1.8 mM or above, and the rate of block at low Ca^{2+} (0.25 mM) was exceedingly slow (Fig. 6*A*). On the other hand, block of G45C channels by 1 μM Cd^{2+} was rapid and readily reversible (Fig. 6*B*), with blockade rates consistent with unimpeded access. The rate of Cd^{2+} blockade in G45C hemichannels was determined at different extracellular Ca^{2+} concentrations from the dominant fast current decay component observed exclusively in oocytes expressing G45C mutant hemichannels (at low Ca^{2+} concentrations, sometimes a slow current decay component like that in wild-type Cx26 hemichannels was present). To evaluate whether Cd^{2+} accessibility correlated with hemichannel opening at different Ca^{2+} concentrations, the blockade rates were plotted for comparison with the normalized current values obtained at different Ca^{2+} concentrations (Fig. 6*C*). The rate of Cd^{2+} block was not significantly changed over a large range of Ca^{2+} concentrations. There was a slight drop in the block rate as the Ca^{2+} concentration increased to 3.5 mM. As previously shown in Fig. 5, the relative open probability of G45C hemichannels is strongly Ca^{2+}-dependent (Fig. 6*C*, black line), so one would expect a tight correlation between the rate of block and hemichannel opening if the physical or electrostatic gate was external to the site of the block. In contrast, the data show that Cd^{2+} was able to access G45C even when hemichannel opening was greatly reduced. These results indicate that the Ca^{2+}-gating ring does not serve as a tight gate that prevents access of ions or even small molecules to the inner pore; the gate must be located below position G45.

Discussion

Although it is well-known that changes in the extracellular Ca^{2+} concentration promote the opening or closing of connexin hemichannels, the molecular mechanisms underlying these

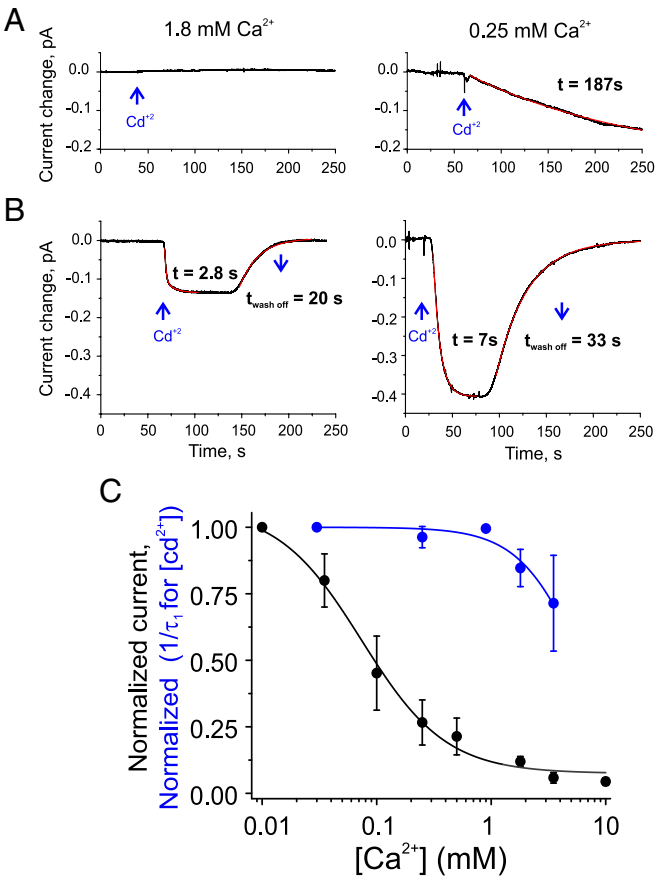

Fig. 6. Cd^{2+} accessibility to G45C is independent of the extracellular Ca^{2+} concentration. (*A*) Normalized holding currents before and after application of 1 μM Cd^{2+} obtained at 1.8 mM (*Left*) and 0.25 mM (*Right*) extracellular Ca^{2+} from different oocytes expressing wild-type Cx26 hemichannels. The red line (*Right*) is a single exponential fit to highlight the slow blockade following Cd^{2+} application. (*B*) Normalized G45C hemichannel holding currents obtained under the same conditions as in *A*. The red lines are exponential fits that show the rapid blockade and unblock of G45C mutant hemichannels after application of 1 μM Cd^{2+} and wash-off, respectively. (*C*) Comparison of the rate of blockade for G45C mutant hemichannels by 1 μM Cd^{2+} (blue circles) and normalized peak tail currents (black circles) as functions of Ca^{2+} concentration. The data represent mean ± SEM of at least three independent measurements.

processes have not yet been solved. We found that conformational changes near the extracellular entrance of the pore, suggested by computational studies and reflected in effects of mutations, are critical for hemichannel gating by Ca^{2+}. These studies support the notion that in Cx26, Ca^{2+} disrupts the intersubunit salt bridge between residues D50 and K61, which consequently affects other electrostatic interactions in this region involving D46, E47, R75, R184, and E187. Experimental data suggest that this electrostatic network of intra- and intersubunit interactions plays critical roles in hemichannel gating reactions. Two negatively charged residues in this region, D50 and E47, might directly interact with Ca^{2+} ions to induce occlusion of the pore. The equivalent residues in Cx46 were shown to have similar roles. D50 and E47 likely form a Ca^{2+}-bound gating ring at the entrance of the pore, as supported by the novel crystal structure of hCx26 gap junction channels obtained in the presence of Ca^{2+} (18). Nevertheless, our accessibility studies show that such a Ca^{2+}-bound gating ring does not prevent access of ions or small molecules to the inner pore, indicating that the gate (physical or electrostatic) is located deeper into the pore.

Previous computational simulations from our group, based on the first crystal structure of human Cx26 gap junction channels (20), which seems to represent the channel with open gates, reveal that K^+ ions accumulate at the extracellular entrance of the aqueous pore (23). Several charged residues in this region (D46, E47, D50, K61, R75, R184) participate in electrostatic networks (21). Those that are negatively charged are pore-lining, which may favor accumulation of permeant cations in this region. In our current work, we replaced six K^+ ions with the same number of Ca^{2+} ions at the entrance of the pore. After equilibration, we found that two of the Ca^{2+} ions rapidly interacted with D50 residues, each in a different subunit.

The simulations showed that following the D50–Ca^{2+} interactions, the electrostatic network near the extracellular end of the pore undergoes significant disruption/rearrangement even within the limited 50-ns simulation time frame. These changes are properly regarded as potential initial changes induced by Ca^{2+} interaction with D50 and the consequent direct disruption of the D50–K61 interaction. Later sequential rearrangements following these initial changes to trigger hemichannel closure were not explored due to time limitations on the current computational methods. It should be noted that the experimentally observed activation and deactivation kinetics in connexin hemichannels and, in particular, for Cx26 hemichannels, occur over many orders of magnitude longer than our simulations. For example, at low Ca^{2+} concentrations (0.01 to 0.1 mM), Cx26 hemichannels display deactivation time constants between 30 and 50 s (17). Nevertheless, the initial events seen in the present simulations indicate that the subsequent rearrangements of the network of electrostatic interactions below D50–K61 are among the steps that enhance the probability of transition to a Ca^{2+}-induced closed state. The previously equilibrated Cx26 hemichannel and other connexin structural models also associate these residues with electrostatic interactions in the open conformation (21, 22).

We further explored the functional roles of residues in this deeper network using mutagenesis. Only a few point mutations led to functional hemichannels (D46C, E47Q, D50N, R184K), but all showed accelerated deactivation kinetics at all extracellular Ca^{2+} concentrations. We previously showed that Cx26 hemichannels deactivate very slowly at low extracellular Ca^{2+} because the electrostatic interaction between D50 and K61 is less likely to be disrupted, which stabilizes the hemichannel in the open state (17, 19). Charge-changing mutations of these residues that weaken the interaction accelerate the closing kinetics (17, 19), similar to results seen with D46C, E47Q, and R184K mutant hemichannels. In addition, in steady-state measurements, mutations of D50 and E47 significantly reduce the apparent affinity for Ca^{2+}, suggesting that they also reduce the ability of Ca^{2+} to stabilize the closed state. A simple interpretation of our previous and present data is that charged residues at the entrance of the pore form an electrostatic network that stabilizes the open hemichannel state in the absence of Ca^{2+}. However, in the presence of Ca^{2+}, this electrostatic network is disrupted/rearranged and two of the negatively charged residues lining the pore, D50 and E47, interact with Ca^{2+} to facilitate the transition to the closed hemichannel state.

The charge-conserving mutation R184K increased the Ca^{2+} sensitivity, whereas one might expect it to have little or no effect. We suggest that its effect is a function of the chemical and structural differences in the side chains. There are substantial differences in the character and configuration of the electrostatic interactions (e.g., number of hydrogen bonds, planar vs. rotational interactions, salt-bridging orientation of the residues) (26). The guanidinium moiety of arginine has a longer length and higher pK_a compared with the butylammonium moiety of lysine (27, 28), and thus one would expect the R184K mutant to establish weaker electrostatic interactions with its anionic partners, including E47 and/or D50. The weaker interactions with nearby negatively charged side chains would allow stronger interactions with Ca^{2+}.

Calculations of salt-bridge interactions show that those involving butylammonium (Lys) moieties have weaker interactions, lower association constants, and a lower probability of binding than those involving guanidinium (Arg) (29). In addition, the geometry of the guanidinium group of arginine enables formation of a larger number of electrostatic interactions compared with lysine (27, 28, 30). Therefore, it is possible that a lysine at position 184 has weaker interactions with other side chains in the open channel conformation, facilitating both Ca^{2+} coordination and disruption of the already-weakened side-chain interactions, increasing the apparent affinity for Ca^{2+}.

Several low-resolution structural methods have shown conformational changes of connexin channels induced by Ca^{2+}. Electron microscopy-based structures of isolated rat liver gap junction channels showed significant differences in pore diameter between Ca^{2+} and Ca^{2+}-free structures (31). Atomic force microscopy of isolated murine Cx26 hemichannels showed an increase in pore diameter from 2.5 to 5 nm when Ca^{2+} is removed, suggesting that Ca^{2+} stabilizes the closed conformation of the channels (32). In this type of preparation, however, Ca^{2+} can access both the extracellular and cytoplasmic domains of the channels, and therefore these studies do not reveal the molecular details and targets of Ca^{2+} interactions. Only one experimental study, from Gómez-Hernández et al. (12), has addressed the putative location of the Ca^{2+} binding site in connexin hemichannels. Using electrophysiological measurements, they showed in Cx32 that mutations of D169 and D178 in the extracellular loops reduce the apparent affinity to extracellular Ca^{2+}. On this basis it was proposed that residue D169 of one subunit and the D178 of an adjacent subunit are arranged precisely to allow interactions with Ca^{2+} (12). However, the residue corresponding to D178 in other connexins strongly regulated by Ca^{2+} is not negatively charged or even a polar residue. Thus, these findings do not address the general mechanism of extracellular Ca^{2+} control of hemichannels.

The recent and novel Ca^{2+}-bound crystal structure for Cx26 gap junction channels showed Ca^{2+} ions located within the pore and coordinated by residues E42, E47, and G45 (18). This only partially agrees with our mutagenesis studies indicating that E47 and D50 are likely part of the binding site in Cx26 hemichannels. This difference could be explained by the different structural rearrangements that occur in connexin hemichannels versus gap junction channels. The docking between the extracellular loops (E1 and E2) of two hemichannels, when forming a gap junction channel between adjacent cells, might significantly restrict movements at the extracellular entrance of the pore that are freely achieved by hemichannels that are undocked.

Importantly, we found that the Cx46 residue D51 (and possibly E48) plays a functional role similar to the analogous residue in Cx26 regarding Ca^{2+} sensitivity, supporting the notion that it is critical in hemichannel Ca^{2+} sensing among different connexin isoforms. More important, when both residues were mutated (E48Q/D51N double mutant), there is a synergistic effect in the decrease of apparent Ca^{2+} affinity. At negative potentials, wild-type Cx46 hemichannels remain closed but the double mutant E48Q/D51N displays large inward currents in response to hyperpolarizing pulses, suggesting that these hemichannels are substantially incapable of being closed even under extreme conditions favoring closure of wild-type channels. The degree of the failure of the double mutant to close was demonstrated by activation of the endogenous Ca^{2+}-activated chloride channels of *Xenopus* oocytes (BAPTA injections eliminated these currents). The simplest interpretation is that E48Q/D51N mutant hemichannels cannot interact significantly with Ca^{2+} at the entrance of the pore or that whatever interaction with Ca^{2+} does occur cannot cause full closure of the pore. Our computational and experimental studies point to interaction of Ca^{2+} with D50 (along with E47) in Cx26 as an initial step in Ca^{2+} gating and the consequent disruption of the intersubunit D50–K61 interaction. However, in Cx46, the residue analogous to K61 is E62, which means that there cannot be a salt-bridge interaction in Cx46 analogous to the D50–K61 interaction in Cx26. Nevertheless, the D51N mutation in Cx46 has a similar effect on Ca^{2+} gating as the D50N mutation in Cx26. This result suggests that the key effect of Ca^{2+} interaction with D50/D51 is disruption of electrostatic interactions in which this residue participates that stabilize the open state, which may be different in different connexins. Nevertheless, the rearrangement of the electrostatic network that follows (involving D46, E47, R75, R184, and E187) is likely to be a general mechanism, because this network is highly conserved between the different connexin types (Fig. S2). Among the negatively charged residues lining the pore in Cx26 and Cx46, E47/E48 and D50/D51 play a major role in Ca^{2+} sensitivity but not the D46/D47 residue. The apparent affinity of the D46C/D47C mutant is the same as that of Cx26 or Cx46 wild type but the mutant D47N in Cx46 has increased Ca^{2+} affinity, indicating that there may be connexin-specific interactions that modulate the general mechanism of divalent sensitivity, as described previously for Cx32 (12).

Recent computational analysis from the Ca^{2+}-bound crystal structure revealed that Ca^{2+} binding produces a positive electrostatic barrier that inhibits occupancy or permeation of cations in the junctional pore (18). Here we tested whether a Ca^{2+}-bound gating ring serves as an electrostatic or physical gate that prevents passage of ions and small molecules in Cx26 hemichannels. We assessed the Ca^{2+} state-dependent accessibility of MTSES and Cd^{2+} to position G45C, which is located below the residues that form the ring. In both cases, the reaction rate for MTSES and the rate of blockade for Cd^{2+} were independent of the extracellular Ca^{2+} concentration. This suggests that the Ca^{2+}-gating ring does not prevent access of atomic ions or molecules the size of MTSES to the inner pore and that the functional gate is located deeper into the pore, below the Ca^{2+}-gating ring and below G45C. The chemical modification rates estimated with MTSES at position G45C were slow (~50 $M^{-1}{\cdot}s^{-1}$). The slow rates for MTSES may be associated with intrinsic properties of the pore that affect reagent accessibility. For example, at the entrance of the Cx26 pore there is a negatively charged ring formed by residues lining the pore that may impede MTSES (a negatively charged reagent) accessibility by electrostatic effects. Unfortunately, MTSET [2-(trimethylammonium)ethyl methanethiosulfonate], which is positively charged, cannot be used at these positions because it has no or little effect on hemichannel conductance (33). When using Cd^{2+}, which is much smaller and highly cationic, to probe accessibility, we observed much faster blockade/modification than with MTSES. Cd^{2+} blockade is achieved with a time constant between 2 and 7 s. Because Cd^{2+} binding is reversible, we cannot directly calculate the on-rate (binding rate) of this reaction from the kinetics of the current blockade; however, if we presume that the Cd^{2+} off-rate (unbinding rate) is independent of the Ca^{2+} concentration, the time constant of Cd^{2+} blockade is a valid index of accessibility to position G45C. Because the blockade time constant does not change over large range of Ca^{2+} concentrations, it is likely that on- and off-rates for Cd^{2+} are not changing.

It is important to note that position G45 is located only two residues deeper than the Ca^{2+}-sensing ring, and was shown to be involved in Ca^{2+} coordination in the recently published Ca^{2+}-bound crystal structure of the Cx26 gap junction channel (18). If this is the case for hemichannels, MTSES or Cd^{2+} would interfere with Ca^{2+} binding to the sensing ring because of competition between these reagents and Ca^{2+} for this site. If so, then the chemical modification rate or rate of current blockade should decrease as we increase the extracellular Ca^{2+} concentration. This does not occur; the rate of modification or blockade does not change significantly over a wide range of Ca^{2+} concentrations. Therefore, we infer that Ca^{2+} binding at the sensing ring does not affect MTSES or Cd^{2+} accessibility to position G45C. This is in agreement with the notion that Ca^{2+} binding in gap junction channels versus hemichannels may involve or produce different structural rearrangements.

Furthermore, it is likely that closure of hemichannels does not require the binding of six Ca^{2+} ions at the entrance of the pore; binding of a smaller number of Ca^{2+} ions, which nevertheless close the pore, may allow access of MTSES and Cd^{2+} deeper into the pore. Allosteric regulation and cooperativity are observed in many ion channels. Indeed, Hill coefficient values 1.38 and 1.75, obtained from the Ca^{2+} dose–response curves for wild-type Cx26 and Cx46, respectively, suggest few sites of Ca^{2+} action and/or cooperativity among different connexin subunits. Further simulations are needed to establish the interplay between the numbers of Ca^{2+} ions at the sensing ring and the ionic and molecular permeability at this region of the pore.

Despite the caveats discussed above for MTSES modification and Cd^{2+} accessibility studies, the combined data strongly support an absence of state-dependent accessibility to position G45C under Ca^{2+} conditions that completely eliminate even ionic conductance, suggesting that the gate is located below this residue. Evidence from other groups suggests that the N-terminal domain, located at the other end of the pore, can form a gate-type plug within the pore (34–36) that is coupled to conformational changes associated with voltage gating (37, 38–40). In the original Ca^{2+}-free crystal structure (20), the N-terminal domain is folded into the intracellular pore entrance and forms hydrophobic interactions with residues of transmembrane segment 1 that line the pore, including position M34. Although it remains elusive to establish whether the N-terminal domain is the primary gate of connexin hemichannels and gap junction channels, this view is not inconsistent with our result suggesting that the gate is located below position G45 and not at the extracellular entrance of the pore. Unfortunately, the N-terminal region in the recent Ca^{2+}-free and Ca^{2+}-bound crystal structures was not resolved (18), leaving unanswered whether conformational changes at this region are produced upon Ca^{2+} binding.

Our data support the notion that the Ca^{2+}-regulatory motifs are located within the ion permeation pathway of connexin hemichannels. This imposes an obligatory structural linkage between gating and permeation not commonly present in other ion channels regulated by Ca^{2+} or other ligands in which the sensors are semiindependent domains distinct from the pore. Several connexin mutation-causing diseases are located in the permeation pathway; therefore, our studies can inform about the mechanism by which these mutations affect gating and permeation, and may help to develop new pharmacological strategies to treat connexin-related diseases.

Materials and Methods

The simulation system was based on the protocol of Luo et al. (23), which included the equilibrated structure of Cx26 in explicit membrane and solvent. CHARMM-GUI (41) was used to construct the Cx26 system, including the membrane and solvent. The system was initially neutralized with Cl^-, followed by addition of K^+ and Cl^- to yield a concentration of 0.1 M KCl (51 K^+ and 105 Cl^- in total). The Cx26 hexamer was solvated in a fully hydrated 1-palmitoyl-2-oleoylphosphatidylcholine (POPC) bilayer (360 POPC molecules) with a 15-Å layer of explicit water above and below the bilayer. The total number of atoms was 180,822. In the simulations, the channel is aligned along the *z* axis/membrane normal from −47 to 47 Å (cytoplasmic to extracellular end of the pore). CHARMM parameter sets were used throughout, including the CHARMM22/CMAP parameters for the protein and ions (42, 43), additive C36 all-atom parameters for lipids (44), and TIP3P for water (45). All systems were simulated with a 1-fs time step using the particle mesh Ewald (PME) method (46) for electrostatics and a Lennard-Jones (LJ) switching function for van der Waals interactions (47). The PME real space and LJ cutoff was 12 Å, the corresponding default value for the parameter sets. Orthorhombic periodic boundary conditions were used for all simulations in the isobaric–isothermal ensemble (also called NpT ensemble) using a Langevin thermostat and Andersen–Hoover barostat. The pressure and temperature were maintained at 1 atm and 300 K, respectively (48). NAMD version 2.9 (49) was used in the simulations. For simulation with Ca^{2+} ions, six K^+ ions near the extracellular pore entrance were replaced by Ca^{2+} ions, and K^+ ions far from the channel were deleted to maintain electroneutrality. The initial positions of the six Ca^{2+} ions were chosen manually to replace the six K^+ ions that were closest to the extracellular entrance at the beginning of the simulation.

For more details, see *SI Materials and Methods*.

ACKNOWLEDGMENTS. We thank Ms. Yu Liu for technical support and Dr. Xuhui Tong for preliminary results. The research reported in this publication was supported by NIH/National Institute of General Medical Sciences Grants R01-GM099490 (to J.E.C.) and R01-GM101950 (to A.L.H. and J.E.C.) and the Health Resources and Services Administration through Grant D34HP26020 to the New Jersey Medical School Hispanic Center of Excellence (to support J.E.C.).

1. Wang N, et al. (2013) Paracrine signaling through plasma membrane hemichannels. *Biochim Biophys Acta* 1828(1):35–50.
2. Sáez JC, Leybaert L (2014) Hunting for connexin hemichannels. *FEBS Lett* 588(8): 1205–1211.
3. García IE, et al. (2015) Keratitis-ichthyosis-deafness syndrome-associated Cx26 mutants produce nonfunctional gap junctions but hyperactive hemichannels when co-expressed with wild type Cx43. *J Invest Dermatol* 135(5):1338–1347.
4. Xu J, Nicholson BJ (2013) The role of connexins in ear and skin physiology—Functional insights from disease-associated mutations. *Biochim Biophys Acta* 1828(1):167–178.
5. Martínez AD, Acuña R, Figueroa V, Maripillan J, Nicholson B (2009) Gap-junction channels dysfunction in deafness and hearing loss. *Antioxid Redox Signal* 11(2): 309–322.
6. Cea LA, et al. (2013) De novo expression of connexin hemichannels in denervated fast skeletal muscles leads to atrophy. *Proc Natl Acad Sci USA* 110(40):16229–16234.
7. Gonzalez JP, Ramachandran J, Xie LH, Contreras JE, Fraidenraich D (2015) Selective connexin43 inhibition prevents isoproterenol-induced arrhythmias and lethality in muscular dystrophy mice. *Sci Rep* 5:13490.
8. Contreras JE, et al. (2004) Role of connexin-based gap junction channels and hemichannels in ischemia-induced cell death in nervous tissue. *Brain Res Brain Res Rev* 47(1–3):290–303.
9. Beahm DL, Hall JE (2002) Hemichannel and junctional properties of connexin 50. *Biophys J* 82(4):2016–2031.
10. Contreras JE, Sáez JC, Bukauskas FF, Bennett MV (2003) Gating and regulation of connexin 43 (Cx43) hemichannels. *Proc Natl Acad Sci USA* 100(20):11388–11393.
11. Ebihara L, Liu X, Pal JD (2003) Effect of external magnesium and calcium on human connexin46 hemichannels. *Biophys J* 84(1):277–286.
12. Gómez-Hernández JM, de Miguel M, Larrosa B, González D, Barrio LC (2003) Molecular basis of calcium regulation in connexin-32 hemichannels. *Proc Natl Acad Sci USA* 100(26):16030–16035.
13. Paul DL, Ebihara L, Takemoto LJ, Swenson KI, Goodenough DA (1991) Connexin46, a novel lens gap junction protein, induces voltage-gated currents in nonjunctional plasma membrane of *Xenopus* oocytes. *J Cell Biol* 115(4):1077–1089.
14. Zampighi GA, Loo DD, Kreman M, Eskandari S, Wright EM (1999) Functional and morphological correlates of connexin50 expressed in *Xenopus laevis* oocytes. *J Gen Physiol* 113(4):507–524.
15. Valiunas V, Weingart R (2000) Electrical properties of gap junction hemichannels identified in transfected HeLa cells. *Pflugers Arch* 440(3):366–379.
16. Ripps H, Qian H, Zakevicius J (2004) Properties of connexin26 hemichannels expressed in *Xenopus* oocytes. *Cell Mol Neurobiol* 24(5):647–665.
17. Lopez W, Gonzalez J, Liu Y, Harris AL, Contreras JE (2013) Insights on the mechanisms of Ca(2+) regulation of connexin26 hemichannels revealed by human pathogenic mutations (D50N/Y). *J Gen Physiol* 142(1):23–35.
18. Bennett BC, et al. (2016) An electrostatic mechanism for Ca(2+)-mediated regulation of gap junction channels. *Nat Commun* 7:8770.
19. Lopez W, Liu Y, Harris AL, Contreras JE (2014) Divalent regulation and intersubunit interactions of human connexin26 (Cx26) hemichannels. *Channels (Austin)* 8(1):1–4.
20. Maeda S, et al. (2009) Structure of the connexin 26 gap junction channel at 3.5 Å resolution. *Nature* 458(7238):597–602.
21. Kwon T, et al. (2012) Molecular dynamics simulations of the Cx26 hemichannel: Insights into voltage-dependent loop-gating. *Biophys J* 102(6):1341–1351.
22. Kwon T, Harris AL, Rossi A, Bargiello TA (2011) Molecular dynamics simulations of the Cx26 hemichannel: Evaluation of structural models with Brownian dynamics. *J Gen Physiol* 138(5):475–493.
23. Luo Y, Rossi AR, Harris AL (2016) Computational studies of molecular permeation through connexin26 channels. *Biophys J* 110(3):584–599.
24. Tong X, et al. (2015) Glutathione release through connexin hemichannels: Implications for chemical modification of pores permeable to large molecules. *J Gen Physiol* 146(3):245–254.
25. Sánchez HA, Mese G, Srinivas M, White TW, Verselis VK (2010) Differentially altered Ca^{2+} regulation and Ca^{2+} permeability in Cx26 hemichannels formed by the A40V and G45E mutations that cause keratitis ichthyosis deafness syndrome. *J Gen Physiol* 136(1):47–62.
26. White AD, et al. (2013) Free energy of solvated salt bridges: A simulation and experimental study. *J Phys Chem B* 117(24):7254–7259.
27. Donald JE, Kulp DW, DeGrado WF (2011) Salt bridges: Geometrically specific, designable interactions. *Proteins* 79(3):898–915.

28. Borders CL, Jr, et al. (1994) A structural role for arginine in proteins: Multiple hydrogen bonds to backbone carbonyl oxygens. *Protein Sci* 3(4):541–548.
29. Debiec KT, Gronenborn AM, Chong LT (2014) Evaluating the strength of salt bridges: A comparison of current biomolecular force fields. *J Phys Chem B* 118(24):6561–6569.
30. Sokalingam S, Raghunathan G, Soundrarajan N, Lee SG (2012) A study on the effect of surface lysine to arginine mutagenesis on protein stability and structure using green fluorescent protein. *PLoS One* 7(7):e40410.
31. Unwin PN, Ennis PD (1983) Calcium-mediated changes in gap junction structure: Evidence from low angle X-ray pattern. *J Cell Biol* 97:1459–1466.
32. Müller DJ, Hand GM, Engel A, Sosinsky GE (2002) Conformational changes in surface structures of isolated connexin 26 gap junctions. *EMBO J* 21:3598–3607.
33. Kronengold J, Trexler EB, Bukauskas FF, Bargiello TA, Verselis VK (2003) Single-channel SCAM identifies pore-lining residues in the first extracellular loop and first transmembrane domains of Cx46 hemichannels. *J Gen Physiol* 122(4):389–405.
34. Oshima A, et al. (2011) Asymmetric configurations and N-terminal rearrangements in connexin26 gap junction channels. *J Mol Biol* 405(3):724–735.
35. Oshima A, Tani K, Hiroaki Y, Fujiyoshi Y, Sosinsky GE (2007) Three-dimensional structure of a human connexin26 gap junction channel reveals a plug in the vestibule. *Proc Natl Acad Sci USA* 104(24):10034–10039.
36. Oshima A, Tani K, Hiroaki Y, Fujiyoshi Y, Sosinsky GE (2008) Projection structure of a N-terminal deletion mutant of connexin 26 channel with decreased central pore density. *Cell Commun Adhes* 15(1):85–93.
37. Verselis VK, Ginter CS, Bargiello TA (1994) Opposite voltage gating polarities of two closely related connexins. *Nature* 368(6469):348–351.
38. Bukauskas FF, Verselis VK (2004) Gap junction channel gating. *Biochim Biophys Acta* 1662(1–2):42–60.
39. Ek Vitorín JF, Pontifex TK, Burt JM (2016) Determinants of Cx43 channel gating and permeation: The amino terminus. *Biophys J* 110(1):127–140.
40. Kronengold J, Srinivas M, Verselis VK (2012) The N-terminal half of the connexin protein contains the core elements of the pore and voltage gates. *J Membr Biol* 245(8):453–463.
41. Jo S, Kim T, Iyer VG, Im W (2008) CHARMM-GUI: A web-based graphical user interface for CHARMM. *J Comput Chem* 29(11):1859–1865.
42. MacKerell AD, et al. (1998) All-atom empirical potential for molecular modeling and dynamics studies of proteins. *J Phys Chem B* 102(18):3586–3616.
43. Mackerell AD, Jr, Feig M, Brooks CL, III (2004) Extending the treatment of backbone energetics in protein force fields: Limitations of gas-phase quantum mechanics in reproducing protein conformational distributions in molecular dynamics simulations. *J Comput Chem* 25(11):1400–1415.
44. Klauda JB, et al. (2010) Update of the CHARMM all-atom additive force field for lipids: Validation on six lipid types. *J Phys Chem B* 114(23):7830–7843.
45. Jorgensen WL, Chandrasekhar J, Madura JD, Impey RW, Klein MLK (1983) Comparison of simple potential functions for simulating liquid water. *J Chem Phys* 79:926–935.
46. Darden T, York D, Pedersen L (1993) Particle mesh Ewald: An *N*·log(*N*) method for Ewald sums in large systems. *J Chem Phys* 98(12):10089–10092.
47. Steinbach PJ, Brooks BR (1994) New spherical-cutoff methods for long-range forces in macromolecular simulation. *J Comput Chem* 15(7):667–683.
48. Feller SE, Zhang Y, Pastor RW, Brooks BR (1995) Constant pressure molecular-dynamics simulation: The Langevin piston method. *J Chem Phys* 103(11):4613–4621.
49. Phillips JC, et al. (2005) Scalable molecular dynamics with NAMD. *J Comput Chem* 26(16):1781–1802.